WESPAC IX 2006

Proceedings of the 9th Western Pacific Acoustics Conference
Seoul, Korea, June 26-28, 2006

Fluid-Structure-Acoustic Analysis of a Polygon Motor

Osamu AKIYAMA, Naoki WATANABE
Quality Assurance Operations
Konica Minolta Business Technologies, Inc., Japan
E-mail: osamu.akiyama@konicaminolta.jp

Takuya YOSHIMURA
Department of Mechanical Engineering
Tokyo Metropolitan University, Japan

Chisachi KATO
Institute of Industrial Science
The University of Tokyo, Japan
E-mail: ckato@iis.u-tokyo.ac.jp

Masashi MIYAZAWA

ABSTRACT

A polygon motor consists of several mirror faces and it is one of the core components for a laser beam printer and a copier. Under high-speed rotation, aeroacoustic noise with a peak frequency of rotational speed times the number of mirror faces and its harmonics is prominently generated from a polygon motor covered with a casing. This paper describes a method to predict such noise that is generated from the flow in between the rotating mirror and stationary casing, propagates through the casing and is radiated into the ambient air. The unsteady flow is firstly computed by large-eddy simulation. The computed pressure fluctuations on the inner wall of the casing are then fed to structural analysis based on a dynamic explicit finite element method that computes the propagation of the elastic waves in the casing. Resulting external surface velocities are finally used for the computation of the acoustical field. A good correlation between the computed and measured results has been observed both in terms of velocity spectra on the casing and spatial distribution of sound pressure level. The proposed method thus seems a promising engineering tool for predicting and identifying the generation mechanism of such noise that is generated from unsteady flow, propagates through solid walls and is radiated to ambient air, in general.

KEYWORDS: Structural Noise, Polygon Motor, Aeroacoustic, Large Eddy Simulation

INTRODUCTION

A rotating polygon mirror reflects laser beam and plots a latent image on a photo conductor drum. A polygon motor generates peak noise at a frequency of nz (n : rotational frequency, z : number of mirror faces) and its harmonics similarly to turbomachinery noise at the blade passing frequency. For high-speed operation of a polygon motor, reduction in the peak noise is demanded although the noise level is not necessarily high when it is covered with a casing. This is because such a peak noise has, in general, a high frequency such as ten

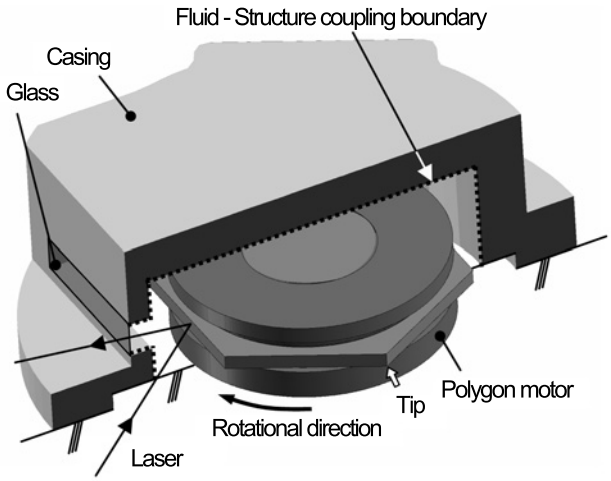

Fig. 1 Polygon motor

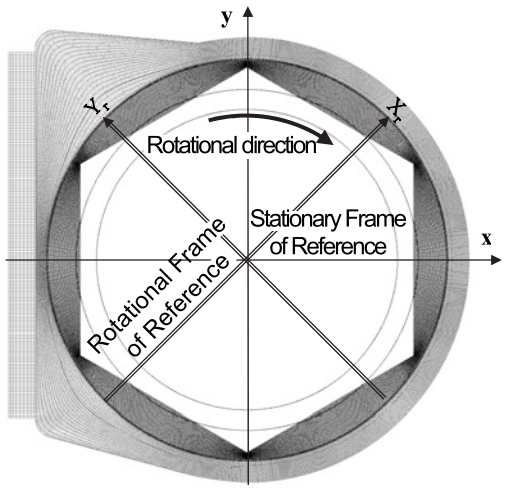

Fig. 2 Computational mesh for the polygon motor

thousand hertzs and is very uncomfortable.

The mechanism of noise generation is roughly described as follows: 1) rotating polygon mirror faces generates pressure fluctuations on the internal surface of the casing, 2) sound waves generated by the vibration source propagates through the solid casing, and 3) vibration velocity on the external surface radiates sound wave into the ambient air. Regarding the flow-induced noise inside a structure like this case, a prediction method based on an one-way coupling analysis of fluid flow, structural and acoustical computations has been applied to a 5-stage centrifugal pump [1, 2, 3, 4].

In this paper is, pressure fluctuations are computed by large-eddy simulation (LES), frequency transfer characteristics and operational deflection shape radiating noise are then computed by dynamic explicit structural analysis, and finally radiated sound fields are predicted by acoustical analysis. Prediction accuracy of the present method is verified by comparisons with measurements in terms of the vibration velocity as well as the radiated sound pressure level (SPL). In addition, sound generating mechanism and propagation characteristic are clarified by the computed results.

INNER FLOW-FIELD COMPUTATION USING LES

Numerical Method and Computational Conditions Pressure fluctuations in the casing are computed by Front Flow - Blue [5, 6], which is an LES code based on a streamline upwind finite element formulation of second order both in time and space and numerically computes the incompressible filtered Navier-Stokes equations. A detailed description is given by Kato et al [7, 8].

The computed polygon motor model sealed with casing and glass is shown in figure 1. It is composed of 6 mirror faces with a tip diameter $D_t = 42.7$ mm that rotates at 63,000 min^{-1}, resulting in a tip speed of $U_t = 141$ m/s. The Reynolds number based on this tip speed U_t and the representative diameter D_t is $Re = 3.98 \times 10^5$. The computational region that is composed of a combination of rotational and stationary frames of reference is depicted with the computational mesh as shown in figure 2. Each mesh includes appropriate margins of overlap with its neighboring mesh upstream and downstream. At every time step, the velocity components and static pressure within such a margin are the values interpolated in the computational mesh of the corresponding neighbor. The number of grid points is approximately 1 million for a mirror face and 5 million in total. The time increment Δt of the computation was set such that 4,000 time steps corresponded to one revolution of the polygon motor ($\Delta t = 7.85 \times 10^{-4}$ [-]).

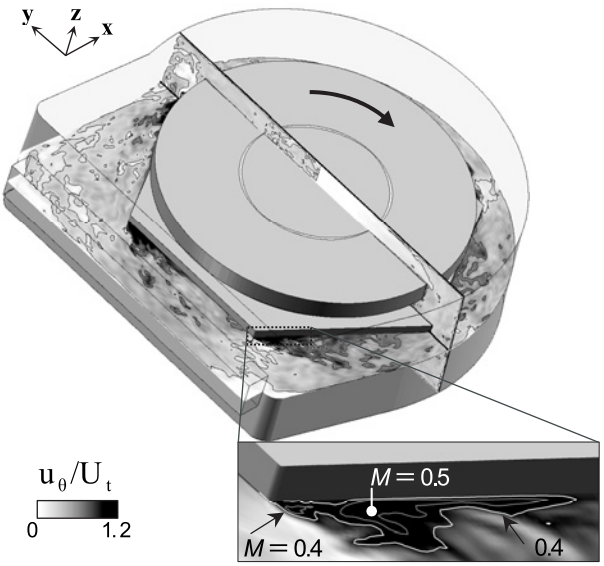

Fig. 3 Computed instantaneous distributions of tangential velocity in the polygon motor's mid-height and x=0 planes

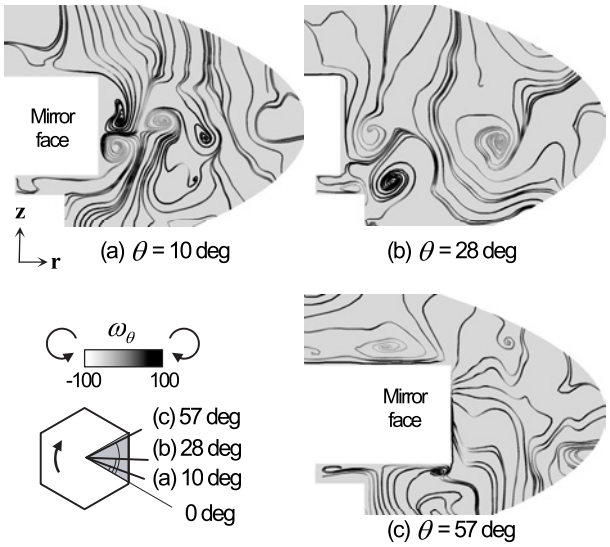

Fig. 4 Computed instantaneous streamlines on θ = 10, 28, 57 degree planes grey-scaled by vorticity ω_θ

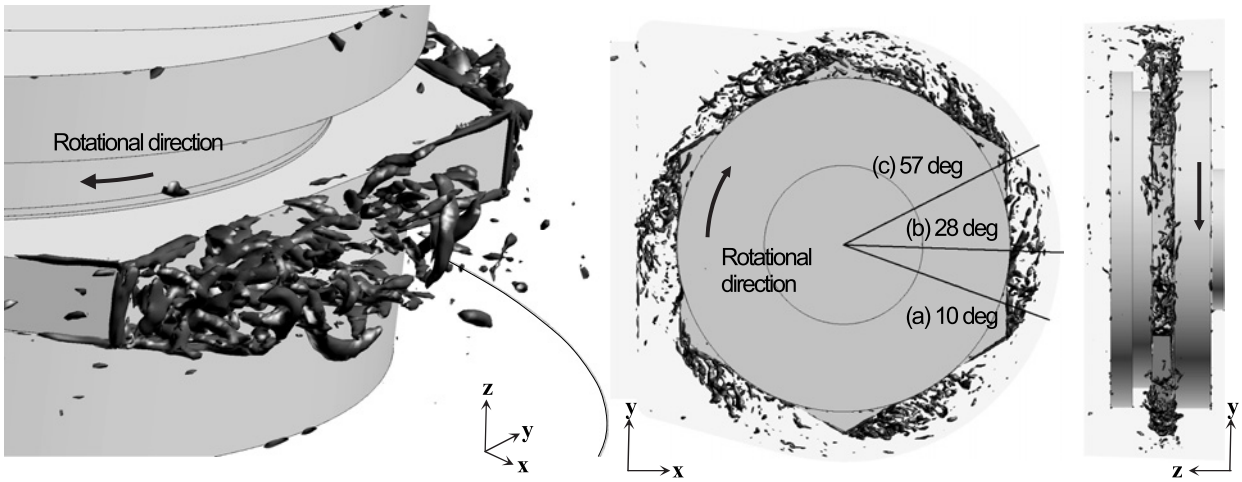

Fig. 5 Computed instantaneous vortical structures around the mirror ($\nabla^2 p$ =1000)

Numerical Results Figure 3 shows the computed instantaneous distributions of tangential velocity. This confirms that flow velocity in downstream of a tip is locally fast ($u_\theta / U_t = 1.53$) due to the recirculating flow downstream of the tip. The detail view near a tip is shown in figure 3 with Mach number contours. The Mach number in the reverse flow region is 0.4 or above and reaches to a local maximum value of 0.64. However, the effect of compressibility is presumably ignorable because such a high Mach number region is localized with a small area and the entire computational domain is also comparatively small.

Figure 4 shows the computed instantaneous streamlines on θ = (a) 10 deg, (b) 28 deg and (c) 57 deg planes. Streamlines are plotted together with tangential direction component vorticity ω_θ indicated by gray scale. In the (a) 10 degree plane, flows separated at the edge of the upper and lower surfaces come into the above-mentioned recirculating zone and form intense vortices there. In the (b) 28 degree plane, some vortices are still generated, but most of the vorticites generated upstream have been and are being destroyed without spreading to radial direction. In the (c) 57 degree plane, all the intense vortices have been destroyed. It can be said that vortical motion has no apparent effects on the downstream mirror.

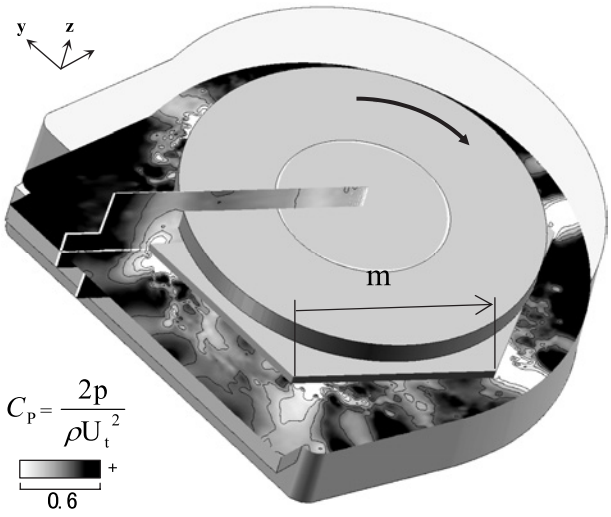

Fig. 6 Computed instantaneous pressure distributions in the mid-height and θ = constant planes

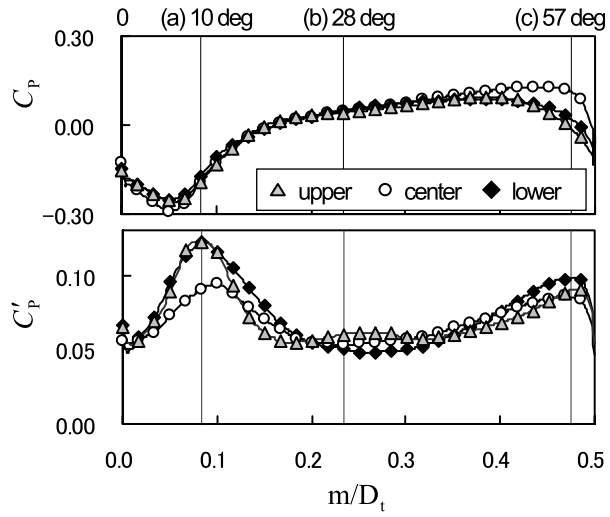

Fig. 7 Computed time-averaged (upper) and fluctuating (bottom) pressure on a mirror face

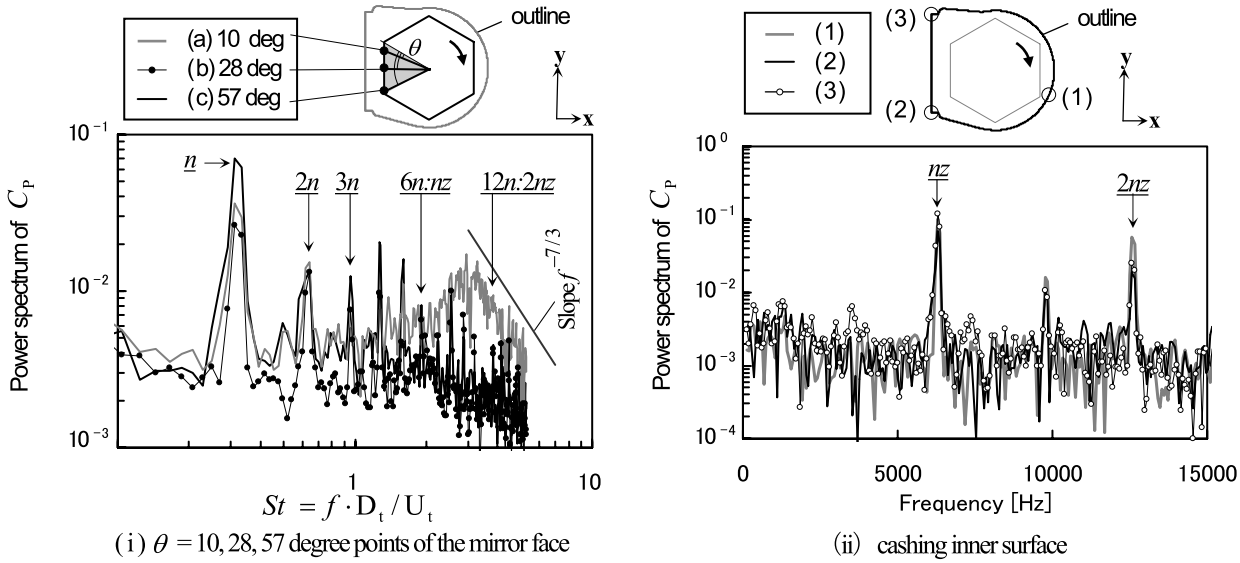

Fig. 8 Computed power spectra of pressure fluctuations

Figure 5 shows the computed instantaneous vortical structures around the mirror with iso-surface of $\nabla^2 p$=1000. As already mentioned, three-dimension vortical structures generated behind a tip are destroyed without spreading to the axial and radial directions. The turbulent vortical motion thus has a limited effect behind a tip and no effect on the other place such as inner casing or downstream mirror faces.

Figure 6 shows the computed instantaneous pressure distributions. Negative pressure regions (relatively low level of pressure region) lie behind a tip, expand to the radial direction and reach to the inner casing surface. When it is viewed from the stationary frame, the pressure difference between the front and rear side of a tip generates fluctuating component at *nz* frequency on the inner surface of the casing.

To focus on the mirror face, better understanding of the pressure field can be obtained by viewing it from the rotating frame. Figure 7 depicts the computed time-averaged and fluctuating pressure on a mirror face. These statistical values are obtained by using flow fields on the six mirror faces during the last three rotations. The three lines show the upper, center and lower distributions against the m-axis shown in figure 6. In the time-averaged pressure C_P, the negative pressure region behind a tip ($m/D_t < 0.15$) corresponds to the

reverse flow region ($M \geq 0.4$ in figure 3). In the fluctuating pressure C'_p, the maximum point located at upper and lower position of $m/D_t = 0.09$ is identical to the θ=10 degree place shown in figures 4 and 5. This indicates that those vortices originating from the separated flows at the upper and lower surfaces cause the intense pressure fluctuation around $m/D_t = 0.09$ shown in figure 7. Figure 8 (i) depicts the computed power spectra of pressure fluctuation at θ= 10, 28 and 57 degree points of the mirror face. The rotational frequency n and its harmonics have a prominent peak. Note here that $6n$, $12n$ components are not dominant as compared with other harmonics components. At θ=10 degree point, where vortical motion is most activated as mentioned above, the computed power spectrum of the fluctuating pressure in the range St= 3 - 5 closely obeys what is expected for the inertial subrange of turbulence. This implies that the important vortical motion is appropriately computed by the present LES.

Figure 8 (ii) plots the computed power spectra of pressure fluctuations at point (1) - (3) in the casing inner surface (in the stationary reference frame). The frequency characteristic of sound source has a prominent peak at nz and $2nz$ components. Note here that nz component is greater than $2nz$ one. The feature is identified not only at these three points, but also at other points.

WAVE PROPAGATION ANALYSIS IN A CASING

Dynamic Explicit Finite Element Method Elastic wave propagation in the casing is computed by NEXST-Impact [9], which is a structural analysis code based on a dynamic explicit finite element method. The structural analysis treats computed pressure fluctuations mentioned in the preceding chapter as excitation forces. Equation of motion for dynamic elastic vibrations of structure is expressed as,

$$[\mathrm{M}]\{\ddot{x}\}+[\mathrm{C}]\{\dot{x}\}+[\mathrm{K}]\{x\}=\{f\} \tag{1}$$

$$[\mathrm{C}]=c_{\mathrm{k}}[\mathrm{K}]+c_{\mathrm{m}}[\mathrm{M}] \tag{2}$$

where $\{x\}$, $\{\dot{x}\}$ and $\{\ddot{x}\}$ are the displacement, velocity and acceleration vectors, respectively. [M] , [C] and [K] are the mass, damping and stiffness matrices, respectively, and $\{f\}$ is the load vector. Assuming that Rayleigh damping is applicable to the casing, the damping matrix [C] is expressed as Eq. (2) where C_{m} is evaluated through an impact test and the corresponding computation, while C_{k} is assumed to be zero.

Computational Conditions Pressure fluctuations computed by the LES feed the load matrix $\{f\}$ in a form of the time history data [3]. The connection and contact boundary conditions for pairing the flange and basement surface are identified such that the computed natural frequency agrees with the measured one. Figure 9 shows the computational mesh for the structural analysis together with the mapped force boundary condition that is indicated by the gray scale. The aluminum casing model with an outer diameter of 64 mm and wall thickness of 7 mm is composed of approximately 50,000 tetrahedral elements, and the glass part for transmitting laser beam is ignored.

Numerical Results Figure 10 shows the distribution of computed normal velocity at $2nz$ (12.6 kHz). The deflection behavior shown in figure 10 is the same as one of the natural modes computed by an eigen-value analysis although it is not shown here. Figure 11 shows a measured deflection shape of the top of casing at $2nz$ in operation. The measured deflection shape is very similar to the computed one (figure 10). This is the first membrane oscillatory mode that efficiently radiates acoustic noise, in general.

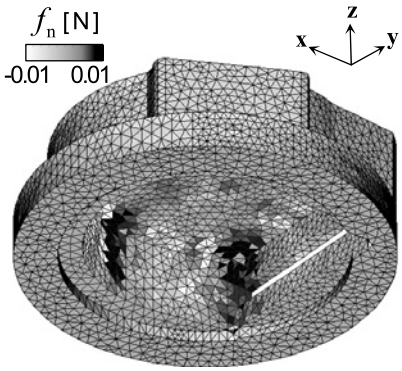

Fig. 9 Computational mesh with force boundary conditions mapped for structural analysis

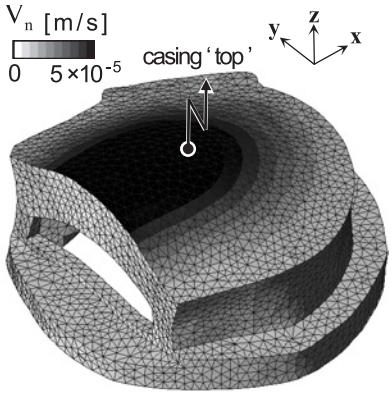

Fig. 10 Distribution of computed normal velocity at 2nz (12.6 kHz)

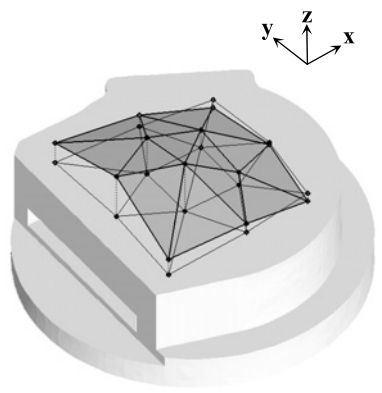

Fig. 11 Measured deflection of the casing top at 2nz (12.6 kHz) in operation

Figure 12 shows a comparison of the normal velocity at the top of casing where Power Spectrum Density (PSD) of the measured and computed velocity are plotted. Both computed and measured velocity have the same trend in which magnitude of 2*nz* component is greater than *nz* one. This trend is apparently the results of the propagating characteristics of the structure at 12.0 kHz. Note that the experimental results have several other peaks such as rotational frequency *n* (1050 Hz) and its harmonics components generated due to the imbalance of the rotor weighted, and 8*n* (8.4 kHz) component excited by the motor coil that are not considered in the present computational model. Although the viscous damping is most likely to be dependent on the place as well as on the frequency, it is treated as a single constant C_m in the present study. A more sophisticated model of the viscous damping will perhaps improve the prediction accuracy in the future.

ACOUSTICAL ANALYSIS OF SOUND FIELD

Numerical Method and Computational Conditions Sound fields are predicted in the frequency domain by a commercial acoustical analysis code SYSNOISE using a boundary element method for the Helmholtz equations [10,11,12]. By applying the particle velocity computed on the external surface of the casing by the structural analysis, is computed at an arbitrary monitor point in a semi-sphere. The computational mesh for the acoustical computation is composed of approximately 5,000 three-node triangle elements with a relatively high resolution where six or more elements are used per wave length of the sound. All reflection condition is given on the z = 0 plane in order to model sound radiation in a semi-anechoic room where the measurement was made. The velocity distributions computed by the structural analysis are transferred to the acoustical mesh shown in figure 13. SPL is computed on a hemisphere at r = 1.0 m distance.

Numerical Results Figure 14 compares the predicted and measured SPL at monitor point 10 (r = 1.0 m point in the z-direction). Note here that the predicted SPL has a different frequency resolution from that in the measurement and therefore its level is adjusted to compensate this difference. As already mentioned, polygon motor noise was measured in a semi-anechoic room with a set of non-directivity microphones in conformity with ISO3746. The present computation successfully predicts that 2*nz* component is greater than *nz* component and dominates the overall noise level although the computed absolute values of these two peak components are 10 - 20 dB lower than the measured equivalents. Regarding the broadband component, the slope around the 2*nz* peak (at 12.6 kHz), which is mainly the results of the structural characteristics, are quantitatively predicted by the present computation. As already mentioned, other peak components are produced by

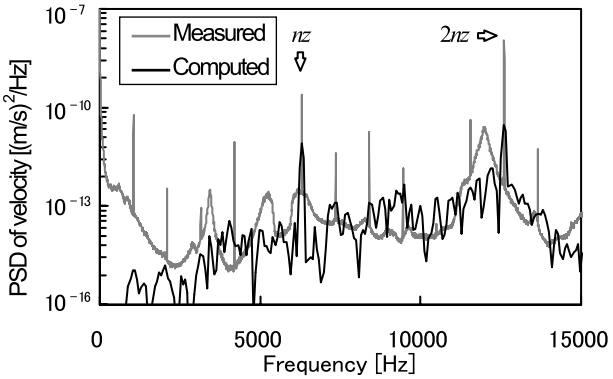

Fig. 12 Comparison of normal velocity at the top of casing

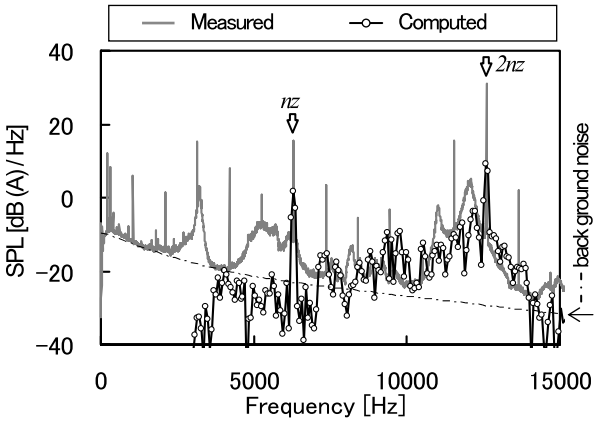

Fig. 14 Comparison of sound pressure level at monitor point 10 (case top- direction, 1.0 m)

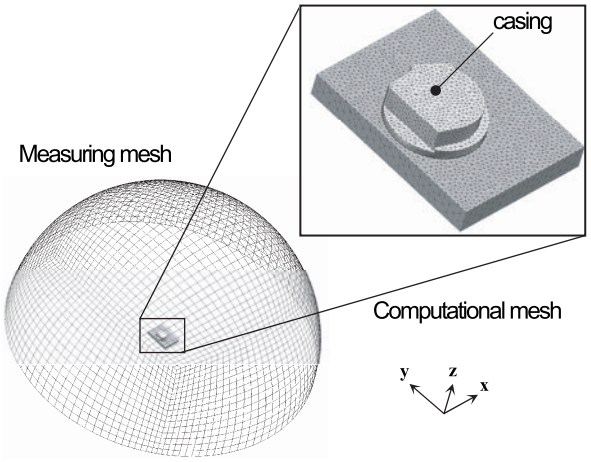

Fig. 13 Computational mesh used for acoustical analysis based on BEM

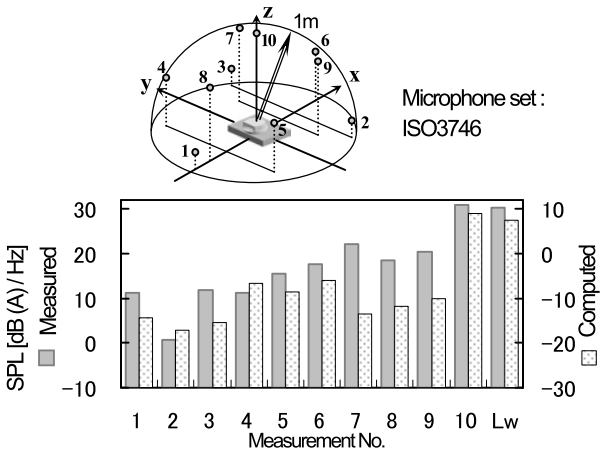

Fig. 15 Comparison of sound pressure level at several measurement points (2nz:12.6 kHz)

what is not modeled in the present study and thus not predicted. Figure 15 shows comparisons of the SPL at 2*nz* component at all the monitor points. Note that the measured and computed SPL refer to a different axis, respectively to the left and right axes. Although the computed SPLs are by around 20 dB lower than the measured ones, the directivity of the sound radiation where intense sound is radiated to the upward direction is reasonably well predicted.

The principal mechanism of sound radiation is then the 1st membrane oscillatory mode of the casing that is excited by the 2nd harmonics of the fluctuating pressure generated by the rotating polygon mirror. Both structural and acoustical analyses quantitatively predict the broadband component while they underpredict the peak components as shown in figure 12 and 14. The discrepancy is, therefore, attributed to the flow field computation and/or the structural analysis. The structural analysis, however, is more likely to be the cause because it dose not predict those peaks at 3.4 kHz and 5.3 kHz that are confirmed by a hammering test.

Finally, we comment on the acoustical mode inside the casing that was ignored in the present analysis. From the inner diameter 48.4 mm of the casing, the frequency of the fundamental mode is estimated to be around 7.0 kHz. But no strong peak exist neither in the measured vibration velocity nor in the measured sound pressure. Therefore, the internal acoustical mode can be safely neglected in this case. However, this may not be the case for a different number of mirror faces and/or rational speed for which the frequencies of the source fluctuation are different.

CONCLUSIONS

This paper proposes a fluid-structure-acoustic coupling analysis method that is capable of predicting aeroacoustic noise generated from a polygon motor. By comparisons with measurements, accuracy of the proposed method is verified in terms of velocity spectra on the casing and spectrum of SPL of the radiated sound. The method thus seems a promising engineering tool that can be applied to the prediction and reduction of noise generated through a mechanism similar to here in presented.

The following issues should perhaps be considered for possible improvement in the prediction accuracy of the proposed method: 1) a more sophisticated model for viscous damping used in the structural analysis and 2) inclusions of the effects of the acoustical models that may develop inside the casing.

ACKNOWLEDGEMENTS

The authors gratefully acknowledge the benefit of advice and cooperation from Yoshinobu Yamade of Mizuho Information & Research Institute, Inc. and Dr. Yu Yan Jiang of AdvanceSoft Co., LTD. The computation codes used in this paper, Front Flow-Blue and NEXST-Impact, have been developed by 'Frontier Simulation Software for Industrial Science' project sponsored by the Ministry of Education, Culture, Sports, Science and Technology (MEXT).

REFERENCES

1. C. Kato, "Prediction of the Noise from a Multi-Stage Centrifugal Pump," *ASME FED SM2005*-77312
2. H. Wang, "Large Eddy Simulation of Unsteady Flow in a Centrifugal Pump," *Proceeding of The 3rd International Symposium on Fluid Machinery and Fluid Engineering* (2004), 168-173
3. Y.Y. Jiang, "Numerical Simulation of Fluid-Structure Coupled Vibration-Flow Induced Noise in a Boiler Feed Pump," *Proceedings of The 3rd International Symposium on Fluid Machinery and Fluid Engineering* (2004), 161-167
4. Y. Takano, "Radiated Noise Simulated from a Full-Scale Multi-Stage Centrifugal Pump," *Proceeding of the Twelfth International Congress on Sound and Vibration* (2005), 731
5. C. Kato, "LES of Unsteady Turbulent Wake of a Circular Cylinder using the FEM," *ASME FED*, **117** (1991), 49-56
6. C. Kato, "LES of Unsteady Flow in a Mixed-Flow Pump," *Int. J. of Rotating Machinery*, **9** (2003), 345-151
7. C. Kato, "An Overset Finite-Element Large-Eddy Simulation Method with Application to Turbomachinery and Aeroacoustic," *Transactions of the ASME, Journal of Applied Mechanics*, **70** (2003), 32- 43
8. C. Kato, "Numerical Prediction of Sound Generated from Flows with a Low Mach Number," *Transactions of the Japan Society of Mechanical Engineers*, B , **71**, 711 (2005), 2613-2621 (in Japanese)
9. Oishi, "A Parallel Explicit Finite Element Analysis Based on the Hierarchical Domain Decomposition," *Transactions of the Japane Society for Computational Engineering and Science*, **3** (2001), 131-136 (in Japanese)
10. von Estorff, "Sound Radiation of a Cantilever Plate Comparisons of BEM Results with Experimental Data," *Betech 91, 6th International Conference on Boundary Element Technology* (1991), 147-158
11. J. P. Coyette, "A Refined Boundary Element Technique for Modeling Acoustic Radiation from Complex Structural Models," *17th International Seminar on Modal Analysis* (1992)
12. J. P. Coyette, "Synthesis of Available Boundary Element Formulations for Solving Acoustic and Elasto-Acoustic Problems," *11th International Modal Analysis Conference* (1992)